doi:10.1093/brain/awv008 BRAIN 2015: 138; 875–890 | 875

BRAIN
A JOURNAL OF NEUROLOGY

Dysfunction in endoplasmic reticulum-mitochondria crosstalk underlies SIGMAR1 loss of function mediated motor neuron degeneration

Nathalie Bernard-Marissal,[1,2] Jean-Jacques Médard,[1] Hamid Azzedine[1,3,*] and Roman Chrast[1,4,*]

*These authors contributed equally to this work.

Mutations in Sigma 1 receptor (*SIGMAR1*) have been previously identified in patients with amyotrophic lateral sclerosis and disruption of *Sigmar1* in mouse leads to locomotor deficits. However, cellular mechanisms underlying motor phenotypes in human and mouse with disturbed SIGMAR1 function have not been described so far. Here we used a combination of *in vivo* and *in vitro* approaches to investigate the role of SIGMAR1 in motor neuron biology. Characterization of *Sigmar1*$^{-/-}$ mice revealed that affected animals display locomotor deficits associated with muscle weakness, axonal degeneration and motor neuron loss. Using primary motor neuron cultures, we observed that pharmacological or genetic inactivation of SIGMAR1 led to motor neuron axonal degeneration followed by cell death. Disruption of SIGMAR1 function in motor neurons disturbed endoplasmic reticulum–mitochondria contacts, affected intracellular calcium signalling and was accompanied by activation of endoplasmic reticulum stress and defects in mitochondrial dynamics and transport. These defects were not observed in cultured sensory neurons, highlighting the exacerbated sensitivity of motor neurons to SIGMAR1 function. Interestingly, the inhibition of mitochondrial fission was sufficient to induce mitochondria axonal transport defects as well as axonal degeneration similar to the changes observed after SIGMAR1 inactivation or loss. Intracellular calcium scavenging and endoplasmic reticulum stress inhibition were able to restore mitochondrial function and consequently prevent motor neuron degeneration. These results uncover the cellular mechanisms underlying motor neuron degeneration mediated by loss of SIGMAR1 function and provide therapeutically relevant insight into motor neuronal diseases.

1 Department of Medical Genetics, University of Lausanne, CH-1005 Lausanne, Switzerland
2 Neurodegenerative Studies Laboratory, Brain Mind Institute, Ecole Polytechnique Fédérale de Lausanne (EPFL), CH-1015 Lausanne, Switzerland
3 Institute of Neuropathology, RWTH Aachen University, 52074 Aachen, Germany
4 Department of Neuroscience and Department of Clinical Neuroscience, Karolinska Institutet, 171 77 Stockholm, Sweden

Correspondence to: Nathalie Bernard-Marissal,
Department of Medical Genetics,
Faculty of Biology and Medicine,
University of Lausanne,
Rue du Bugnon 27,
CH-1005 Lausanne,
Switzerland
E-mail: Nathalie.BernardMarissal@unil.ch, Nathalie.Bernard@epfl.ch

Received July 8, 2014. Revised November 29, 2014. Accepted December 2, 2014. Advance Access publication February 12, 2015

Correspondence may also be addressed to: Hamid Azzedine, E-mail: azzedine.hamid@yahoo.fr, hazzeddine@ukaachen.de; or Roman Chrast, E-mail: Roman.Chrast@unil.ch, Roman.Chrast@ki.se

Keywords: Sigma 1 receptor; motor neuron degeneration; MAMs loss; mitochondrial and endoplasmic reticulum dysfunction

Abbreviations: ALS = amyotrophic lateral sclerosis; CHOP = C/EBP homologous protein; ER = endoplasmic reticulum; MAM = mitochondria-associated membrane; PDI = protein disulphide isomerase

Introduction

Motor neuron diseases regroup incurable neurological disorders characterized by the gradual and selective degeneration of motor neurons. Among them, amyotrophic lateral sclerosis (ALS) is the most representative adult motor neuron disease with an incidence rate of 2–3 per 100 000 (Al-Chalabi *et al.*, 2012). Although the familial cases represent only ~10% of all ALS cases, their characterization led to substantial insight into the pathophysiology of ALS (Sreedharan and Brown, 2013). Accumulating evidence from mouse models of motor neuron disease implicated synaptic pathology (Pun *et al.*, 2006), mitochondrial dysfunction (Court and Coleman, 2012), calcium signalling impairment (Bernard-Marissal *et al.*, 2012), endoplasmic reticulum (ER) stress (Saxena *et al.*, 2009) and disturbances of axonal transport (Bilsland *et al.*, 2010) as critical factors involved in motor neuron degeneration in ALS mouse models.

Recently, mutations in SIGMAR1 have been identified in frontotemporal lobar degeneration co-occurring with ALS (FTLD-ALS) (Luty *et al.*, 2010) and in juvenile ALS (Al-Saif *et al.*, 2011). SIGMAR1 is a chaperone protein located at the interface between the ER and mitochondria, called mitochondria-associated membranes (MAMs). These structures have been shown to be involved in the control of lipid biosynthesis, mitochondrial division, calcium signalling and dynamics of the two organelles (Hayashi *et al.*, 2009). At the MAMs, SIGMAR1 regulates the compartmentalization and export of lipids such as cholesterol and galactoceramide as well as the transfer of calcium between ER and mitochondria by chaperoning the inositol 1,4,5-trisphosphate receptor 3 (ITPR3, formerly known as IP3R3). Once activated by IP3, ITPR3 release calcium, which is immediately captured into mitochondria by the voltage-dependent anion channel 1 (VDAC1) (Hayashi and Su, 2007). The knock-down of SIGMAR1 *in vitro* was shown to lead to calcium homeostasis defects and ER stress activation and to enhance apoptosis induced by stress factors (Hayashi and Su, 2007; Prause *et al.*, 2013). The *Sigmar1* knock-out mouse (*Sigmar1*$^{-/-}$) presents motor disabilities as measured by evaluation of spontaneous locomotor activity or by rotarod test (Langa *et al.*, 2003; Mavlyutov *et al.*, 2010). In spinal cord, SIGMAR1 is highly expressed in motor neurons and has been observed at the subsurface cisternae of the ER at the level of large cholinergic postsynaptic densities (Mavlyutov *et al.*, 2010). Crossing *Sigmar1*$^{-/-}$ mice with the ALS mouse model *SOD1*^{G93A} exacerbated the motor phenotype and accelerated the end stage of the disease (Mavlyutov *et al.*, 2013). Conversely, stimulating SIGMAR1 function using the agonists Pre-084 or SA4503 has been shown protective in both *in vitro* and *in vivo* models of motor neuron diseases (Mancuso *et al.*, 2012; Ono *et al.*, 2014).

Although these data strongly suggest a role of SIGMAR1 in motor neurons, the cellular mechanisms leading to motor neuron degeneration in the context of disturbed SIGMAR1 function have not been characterized so far. In the present study, we used *in vivo* and *in vitro* models of loss-of-function of SIGMAR1 to demonstrate the importance of calcium homeostasis, and ER and mitochondrial function regulation for maintenance of motor neuron integrity.

Materials and methods

Animals

We used the previously described *B6;129S5-Sigmar1*$^{Gt(OST422756)Lex}$ knockout mice (*Sigmar1*$^{-/-}$) (Mavlyutov *et al.*, 2010) purchased from MMRRC. Offspring was genotyped by separated PCR using the following primers: wild-typeF 5' TCTGAGTACGTGCTGCTCTTCG 3' and wild-typeR 5'CAGAAATCTCAGCCCAGTATCG3', MTF 5' TCTGAGTACGTGCTGCTCTTCG 3' and MTR 5' ATAAACCCTCTTGCAGTTGCATC 3'. For neuronal cultures, embryos were collected from wild-type and *Sigmar1*$^{-/-}$ mice at gestational Day 12.5 (E12.5) or from rat wild-type (Janvier Labs) at E14. For histological studies animals were sacrificed at 2.5 and 5 months old. Animals were housed in a controlled environment with a 12-h light/12-h dark cycle, with free access to water and standard chow diet. All experiments were performed in accordance with the legal requirements of the University of Lausanne and the Canton de Vaud.

Behavioural studies

Rotarod studies were performed as previously described (Dierssen *et al.*, 2011). Mice (wild-type $n = 8$ and *Sigmar1*$^{-/-}$ $n = 9$ at 2.5 months old and wild-type $n = 6$ and *Sigmar1*$^{-/-}$ $n = 7$ at 5 months old) were placed on the rotating rod and challenged using the following steps: on Days 1 and 2, mice learned to stay on the rotarod at constant speed of 5 rpm for 180 s. At Day 3, motor coordination was assessed on the accelerating rotarod with a rate of 4 to 50 rpm for 2.5 min. For each trial, the time until the mice fall off the rod was recorded. Data were expressed as means ±standard error of the mean (SEM). Muscle strength was measured by modified grid test on 5-month-old wild-type and *Sigmar1*$^{-/-}$ mice as previously described (Saxena *et al.*,

2009). Mice were trained for 4 days before being scored. Their ability to lift grids of 10, 20, 30 and 40 g was measured three times with a maximum duration of 60 s. Trials were separated by 15 s pauses. The best score for each grid was kept. Muscle force values correspond to the sum of times for each grid multiplied by the weight of the grid. Data were expressed as means ± SEM.

Primary cultures

Motor neuron cultures were prepared from E12.5 mice embryos as previously described (Bernard-Marissal *et al.*, 2012). Briefly, cells were dissociated mechanically after trypsin treatment of the dissected spinal cords. The largest cells were isolated using iodixanol density gradient purification. After a final BSA cushion, motor neurons were plated onto poly-ornithine/laminin-coated wells in Neurobasal® medium (Invitrogen) complemented with a mixture of neurotrophic factors (1 ng/ml BDNF, 100 pg/ml GDNF, and 10 ng/ml CNTF), 2% horse serum, B27 supplement (Invitrogen), 0.05 mM L-glutamine, 25 mM glutamate, and 25 mM mercaptoethanol.

Dorsal root ganglia dissociated cultures were performed as previously described (Stendel *et al.*, 2010). Dorsal root ganglia were obtained from E14.5 rat embryos, digested enzymatically (0.25% trypsin-EDTA; Invitrogen) and seeded on polyornithinin/laminin-coated coverslips in Neurobasal® medium containing 4 g/l D-glucose, 2% B27 supplement (Invitrogen), 2 mM L-glutamine and 50 ng/ml NGF.

Rat Schwann cell cultures were prepared as previously described (Stendel *et al.*, 2010). Postnatal Day 3 rat sciatic nerves were dissociated in 4 mg/ml collagenase type 1 (Sigma), 1.2 mg/ml hyaluronidase (Sigma) and 0.3 mg/ml trypsin inhibitor (Sigma) in minimal essential medium at 37°C for 60 min. Subsequently, cells were plated on plastic dishes coated with poly-L-lysine (Sigma) in Dulbecco's modified Eagle medium (DMEM) containing 10% foetal calf serum (FCS), 1% penicillin/streptomycin (Invitrogen) and 10 µM cytosine arabinoside (Sigma). After 24 h, cells were washed and incubated in Schwann cell growth medium [DMEM containing 10% FCS, 4 µg/ml crude glial growth factor (BioReba Biotechnology) and 2 µM forskolin (Sigma)]. Purification of rat Schwann cells to remove fibroblasts was realized using Thy1.1 antibody (AbD Serotec) and rabbit complement (Sigma).

Except for neuronal survival experiments, rat neurons were fixed with paraformaldehyde (PFA 4%) 8 h after treatment or at 16 h after plating for mouse neurons. Neuronal/Schwann cells survival was assayed 24 h after treatment (rat neurons) or seeding (mouse wild-type and *Sigmar1*$^{-/-}$ neurons), respectively by manual counting and also checked after using SMI32 staining (motor neuronal marker).

Immunocytochemistry

Cultured cells were fixed at indicated times with PFA 4% for 20 min at 4°C, then washed three times with phosphate-buffered saline (PBS) and blocked in PBS (2% BSA, 2% heat-inactivated goat serum, and 0.1% Triton™ X-100) for 1 h at room temperature and incubated at 4°C overnight with one of the following primary antibodies: goat anti-sigma 1 receptor 1/150 (L20, Santa Cruz, sc16203), mouse anti-protein disulphide isomerase (PDI) 1/250 (SPA 891, Stressgen), mouse anti-non-phosphorylated neurofilament H (SMI32) 1/500 (Covance), rabbit anti-peripherin 1/1000 (AB1530, Millipore), mouse anti-cytochrome-c 1/500 (6H2.B4, BD Biosciences) rabbit anti-GADD 153 (F-168): sc-575 (CHOP) 1/150 (Santa Cruz), rabbit anti-phospho-eIFa (Ser51) 1/200 (Cell Signaling Technology) and anti-phospho Histone H3 (Ser10) 1/1000 (Santa Cruz). Cells were washed three times with PBS, then incubated with the appropriate secondary antibody (Invitrogen), washed three times with PBS, and launched in VECTASHIELD® mounting medium with DAPI (Vector). Cells were observed under Zeiss Axiovision fluorescence microscope and analysed using either ImageJ or Axiovision v4.8 software.

Proximity ligation assay

After fixation and blocking, neurons were incubated overnight with rabbit anti-IP3R3 (ITPR3) 1/250 (Chemicon) and mouse anti-VDAC1 1/250 (Abcam) or rabbit anti-calreticulin 1/500 (ABR) and mouse anti-NeuN 1/500 (Millipore) primary antibodies. After PBS wash, the proximity ligation assay (PLA) probes anti-rabbit PLUS anti-mouse MINUS were added for 1 h in the antibody diluent buffer. If the two proteins of interest were 40 nm or closer, connector oligonucleotides hybridized with the PLA probes, and after ligation, the signal was amplified by rolling circle amplification. The Duolink® detection fluorophore red excitation/emission = 594/624 nm was used. The fluorescent spots (PLA signals) were analysed using the plugin 'analyze particles' of ImageJ. As a negative control, one of the primary antibodies was omitted, and the PLA probe background staining was analysed. The background staining was limited for both probes.

Calcium imaging

To monitor quantitative changes of $[Ca^{2+}]i$ in motor neurons, we used the ratiometric Fura 2-AM (Life Technologies) indicator probe. Twenty-four hours after seeding, motor neurons were treated or not with NE-100 and monitored by calcium imaging 8 h later. Motor neurons were loaded with Fura-2 (4 µM) in a pH 7.4 solution containing: 150 mM NaCl, 2 mM KCl, 2 mM $MgCl_2$, 2 mM $CaCl_2$, 10 mM HEPES, and 10 mM glucose, for 20 min in the dark at 37°C, the dye was then washed off and the coverslips reincubated in the dark for a further 30 min at room temperature to allow de-esterification of the dye. After loading, coverslips were transferred to an inverted microscope Zeiss Axiovert 200 M. To selectively visualize motor neurons we first used transmitted light and thereafter acquired fluorescent images of Fura 2. Fura 2 was alternately excited at 340 and 380 nm and emission collected at 510 nm. Images were acquired at 2 s intervals with MetaFluor (Molecular Devices) on a ×40 objective.

For $[Ca^{2+}]$ analysis we first drew regions of interest on motor neurons and then used them for analysis of Fura 2 images. $[Ca^{2+}]$ values were presented as the 340/380 nm ratio. During experiments, neurons were perfused continuously with external solution (0.5 ml/min) using a peristaltic pump. To invoke Ca^{2+} influx, 25 mM KCl was applied in external solution (NaCl was replaced with equimolar amounts of KCl) for 20 s. $[Ca^{2+}]i$ levels were calculated from the ratio of fluorescent signals at excitation 340 and 380 nm, and calibrated by sequential addition of saturating $CaCl_2$ (20 mM) and EGTA (20 mM) in external solution after incubation with 10 mM

A23 187 Ca^{2+}-ionophore (Sigma) and then translated to nanomolar using the Grynkiewicz formula (Grynkiewicz *et al.*, 1985). Resting $[Ca^{2+}]c$ was determined as the average ratio value between 30 and 180 s of recording. After KCl application, the cells were perfused with the KCl-free solution for an additional 3 min to let them recover.

Mitochondrial axonal transport

Motor neurons were loaded with 25 nM of MitoTracker® Red CMXRos (Life Technologies) for 15 min at 37°C, then washed with Neurobasal® for 15 min at room temperature. Mitochondria movement was monitored on an inverted Zeiss Axiovert 200 M with a ×63 objective using MetaMorph software (Molecular Devices) and time-lapse imaged every 5 s for 10 min. Time-lapse image stacks of 50 µm axon segments were analysed using the ImageJ plugin Difference Tracker (Andrews *et al.*, 2010). The percentage of moving particles was determined using Difference Filter, which allowed extraction of the moving pixels from the background stationary particles, based on the intensity of pixel (chosen value: 10) and the comparison of a number of offset frames (chosen value: 4). The velocity of the particles was analysed using Mass particle tracker with standard criteria (minimum tracked intensity: 20, minimum feature size: 2, initial flexibility: 10, subsequent flexibility: 5 and minimal track length: 4). As an average, 20–30 axonal segments were analysed per condition. Kymographs of selected axons were realized using the ImageJ macro kymograph tool.

Reagents

For *in vitro* experiments, the following reagents were used: SIGMAR1 antagonist (NE-100), agonist (Pre-084) and Mdivi-1 were purchased from Tocris Biosciences. Thapsigargin was purchased from Calbiochem, tunicamycin and monastrol were from Sigma-Aldrich. salubrinal and 1,2-bis(2-aminophenoxy)ethane-N,N,N,N-tetraacetic acid tetrakis(acetoxymethyl) ester (BAPTA/AM) were from Alexis Corporation and z-Ala-Thr-Ala-Asp(OME)-fmk (z-ATAD-fmk) was acquired from MBL International.

Immunohistochemistry

Mice were anaesthetized with a mixture of 10 µl/g of Ketanarkon 100 (1 mg/ml, Streuli) with 0.1% Rompun® (Bayer) in PBS then perfused transcardially with PBS followed by paraformaldehyde (PFA) 4% in PBS. Spinal cords were dissected out, incubated for 2 h in PFA 4% at 4°C, and then in 25% sucrose in PBS overnight. Tissues were embedded in Optimal Cutting Temperature compound (Tissue-Tek). Eighteen micrometre-thick cryosections were collected onto Superfrost™ Plus slides (Thermo Scientific), washed with PBS, and incubated in the blocking solution (PBS, 4% BSA, 4% heat-inactivated goat or donkey serum, and 0.2% Triton™ X-100) for 1–2 h. Sections were then incubated with the appropriate primary antibodies overnight: rabbit anti-PeiF2a 1/200 (Cell Signaling Technology), mouse anti-non-phosphorylated neurofilament H (SMI32) 1/500 (Covance), rabbit anti-cleaved caspase 3 (Cell Signaling Technology), goat anti-MMP9 1/250 (Sigma-Aldrich) and anti-mouse NeuN 1/500 (Millipore). Spinal cord sections were washed three times with PBS, incubated with the appropriate secondary antibody, washed three times with PBS, and launched in Mowiol® mounting medium. Pictures were taken with a Zeiss Axiovision microscope (Zeiss) using ×20 and ×40 objectives. Immuno-quantification was performed using ImageJ software.

Tibialis anterior and soleus muscles were collected, then post-fixed for 20 min in 4% PFA and incubated in the sucrose solution overnight at 4°C. Twenty-five micrometre sections of tibialis anterior and 15 µm sections of soleus were incubated for 5 h in PBS, 4% BSA, 0.5% Triton™ X-100 and anti-Neurofilament 145 (Millipore) was diluted at 1/200 in the same solution and applied to slices for 2 days. Tissues were washed with PBS, and secondary antibody and α-bungarotoxin CF594 (Biotium) were added at the same time for 2 h. Muscle sections were then washed with PBS including as a final step in water and finally mounted in Mowiol®. Pictures were taken with a Zeiss Axiovision microscope (Zeiss) using ×20 objectives and Z-stacks were performed to quantify the number of denervated, partially innervated (intermediate) and innervated neuromuscular junctions.

Western blot

Western blots were done on lysates from lumbar spinal cord dissected from 2.5-month-old wild-type or *Sigmar1*$^{-/-}$ mice. Samples were lysed in a lysing buffer containing: 50 mM Tris-HCl, pH 7.5, 150 mM NaCl, 2 mM EDTA, 2 mM EGTA, and 1% SDS supplemented with a protease inhibitor mixture (Roche Molecular Biochemical). Protein concentration was determined using the BCA kit (Pierce). Protein samples were separated by SDS-PAGE and blotted to nitrocellulose membranes (Schleicher and Schuell, Whatman International). After blocking in 5% milk, the following primary antibodies were used: mouse anti-SIGMAR1 1/100 (Santa-Cruz) and mouse anti-actin (AC40, 1/20,000; Sigma). After incubation of the blots with horseradish peroxidase (HRP)-conjugated secondary antibodies, proteins were revealed using the chemiluminescent HRP substrate (Millipore). Immunoblot images were quantified using the software ImageJ and normalized relative to actin levels.

Electron microscopy

Animals were perfused with a mixture of 2% PFA and 2% gluteraldehyde in sodium cacodylate buffer (0.1 M). Lumbar spinal cord was collected and post-fixed for 3 h, washed in 0.1 M cacodylate buffer, and osmicated for 4 h in 1% OsO4 (Fluka). Tissues were rinsed in 0.1 M cacodylate buffer, dehydrated and embedded in epoxy 812-Araldite (Polysciences). Ultra-thin sections were subsequently cut, collected on cellodin-coated single slot grids and stained with uranyl acetate and lead citrate. Photographs were obtained using a Tecnai G2 electron microscope. We quantified the number of mitochondria displaying close contacts with ER and expressed it relative to the total number of mitochondria per field.

Statistical analysis

For survival and immune-quantification experiments, differences were evaluated for their statistical significance by two-tailed, unpaired Student's *t*-test. Values were expressed as per cent ± standard error of the mean (SEM). Significance

was accepted as the level of $P < 0.05$ ($^{*}P < 0.05$, $^{**}P < 0.01$, and $^{***}P < 0.001$). For behavioural experiments, statistical significance was evaluated with a non-parametric Mann-Whitney-U test. Values were expressed as the mean ± SEM. Significance was accepted as the level of $P < 0.05$ ($^{*}P < 0.05$).

Results

Loss of SIGMAR1 function leads to neuromuscular dysfunction *in vivo*

As SIGMAR1 dysfunction was shown to affect motor function both in mice and humans, we aimed at determining whether this motor phenotype was related to motor neuron degeneration. We confirmed that *Sigmar1*$^{-/-}$ mice displayed motor coordination defects detected on accelerating rotarod (Supplementary Fig. 1A and B) as previously described by Mavlyutov *et al.* (2010). To assess whether these locomotor defects were linked to muscle weakness, we monitored muscle strength of 5-month-old *Sigmar1*$^{-/-}$ mice using the grid test developed by Saxena *et al.* (2009). Muscle strength of *Sigmar1*$^{-/-}$ mice was significantly lower compared to wild-type mice (Fig. 1A). As muscle weakness is usually connected to muscle denervation in motor neuron disease (Saxena *et al.*, 2009), we analysed the level of neuromuscular junction innervation at different stages. At the age of 2.5 months, ~30% of neuromuscular junctions were partially innervated, and at the age of 5 months, ~20% of neuromuscular junctions were denervated in tibialis anterior (Fig. 1B and C). Interestingly, no difference at the level of neuromuscular junctions between wild-type and *Sigmar1*$^{-/-}$ mice was observed in the slow-twitch muscle, soleus (Supplementary Fig. 1C). The quantification of motor neurons in lumbar spinal cord highlighted a small, but significant, loss of motor neurons in 5-month-old knockout animals (wild-type: 503 ± 23, *Sigmar1*$^{-/-}$: 435 ± 15) (Fig. 1D and E). Motor neuron degeneration was also suggested by presence of cleaved caspase 3-positive motor neurons in *Sigmar1*$^{-/-}$ spinal cord sections (Supplementary Fig. 1D). This low level of motor neuron death may suggest the death of a subpopulation of motor neurons. We therefore analysed the proportion of fast vulnerable motor neurons, which are known to degenerate earlier in the *SOD1*^{G93A} ALS mouse model, based on their expression of MMP9 (Kaplan *et al.*, 2014). The mean number of highly expressing MMP9 motor neurons was significantly decreased in the ventral horn of 5-month-old *Sigmar1*$^{-/-}$ mice (wild-type: 3 ± 0.25, *Sigmar1*$^{-/-}$: 1.8 ± 0.34) indicating that this motor neuronal population may be particularly affected by loss of SIGMAR1 function (Fig. 1F and G).

Loss of SIGMAR1 function leads to motor neuron degeneration *in vitro*

To characterize the underlying cellular mechanisms leading to changes in motor neuron physiology, we cultured primary embryonic motor neurons that have been previously successfully used as a model to identify cellular pathways in motor neuron disease (Bernard-Marissal *et al.*, 2012). In cultured motor neurons, SIGMAR1 was expressed in the soma and processes and co-localized with the ER chaperone protein disulphide isomerase (Supplementary Fig. 1E). To analyse the consequence of SIGMAR1 dysfunction, we seeded motor neurons extracted either from wild-type and *Sigmar1*$^{-/-}$ mouse embryos or wild-type rat embryos treated with a selective antagonist and agonist of SIGMAR1, NE-100 and Pre-084, respectively (Hayashi and Su, 2007). Both NE-100 treated motor neurons and *Sigmar1*$^{-/-}$ motor neurons showed a significant reduction (~20–30%) in axonal length compared to controls (Fig. 2A and B). To ensure that the observed axonal length reduction was the consequence of axonal degeneration rather than a defect in axonal growth, we stained motor neurons with peripherin, which is known to label axonal swellings and spheroids (Corbo and Hays, 1992). We observed a significant increase in the number of large axonal swellings at the end terminals of NE-100-treated motor neurons and *Sigmar1*$^{-/-}$ motor neurons (none: 0.8 ± 0.2, NE-100: 2.15 ± 0.3 $P = 0.013$; wild-type: 1.2 ± 0.3 and *Sigmar1*$^{-/-}$: 3.4 ± 0.4, $P = 0.0003$) (Fig. 2B and C). This axonal degeneration was followed a few hours later by ~40% of motor neuron cell death (Fig. 2D) in both SIGMAR1 dysfunction conditions suggesting a dying-back degeneration. Importantly, treating motor neurons with a specific SIGMAR1 agonist, Pre-084, prevented both axonal degeneration (Fig. 2C) and the death induced by NE-100 (Fig. 2D). Importantly, NE-100 and Pre-084 have no effect on the survival of *Sigmar1*$^{-/-}$ motor neurons, confirming their specificity for SIGMAR1 (Supplementary Fig. 1F). Finally, the observed effect of NE-100 was specific for motor neurons. Indeed, sensory neurons survival was not affected even when treated with higher doses of NE-100 (Fig. 2D).

ER–mitochondria disconnection is observed both in *in vitro* and *in vivo* models of loss of SIGMAR1 function

SIGMAR1 is localized at the outer membrane of the ER at specific contact points between ER and mitochondria called MAMs (Hayashi and Su, 2007). As SIGMAR1 dysfunction has been previously connected to MAM disturbances (Hayashi and Su, 2007), we quantified the level of MAMs in motor neuron cultures. As the distance between ER and mitochondria at MAMs is ~10–20 nm (Csordas *et al.*, 2006), we used an *in situ* proximity ligation assay (De Vos *et al.*, 2012; Hedskog *et al.*, 2013). Cultured motor neurons were probed with anti-ITPR3 (ER side) and anti-VDAC1 (mitochondrial side) primary antibodies followed by hybridization with secondary antibodies coupled to different oligonucleotides that hybridize together if the distance between two antibody-coupled

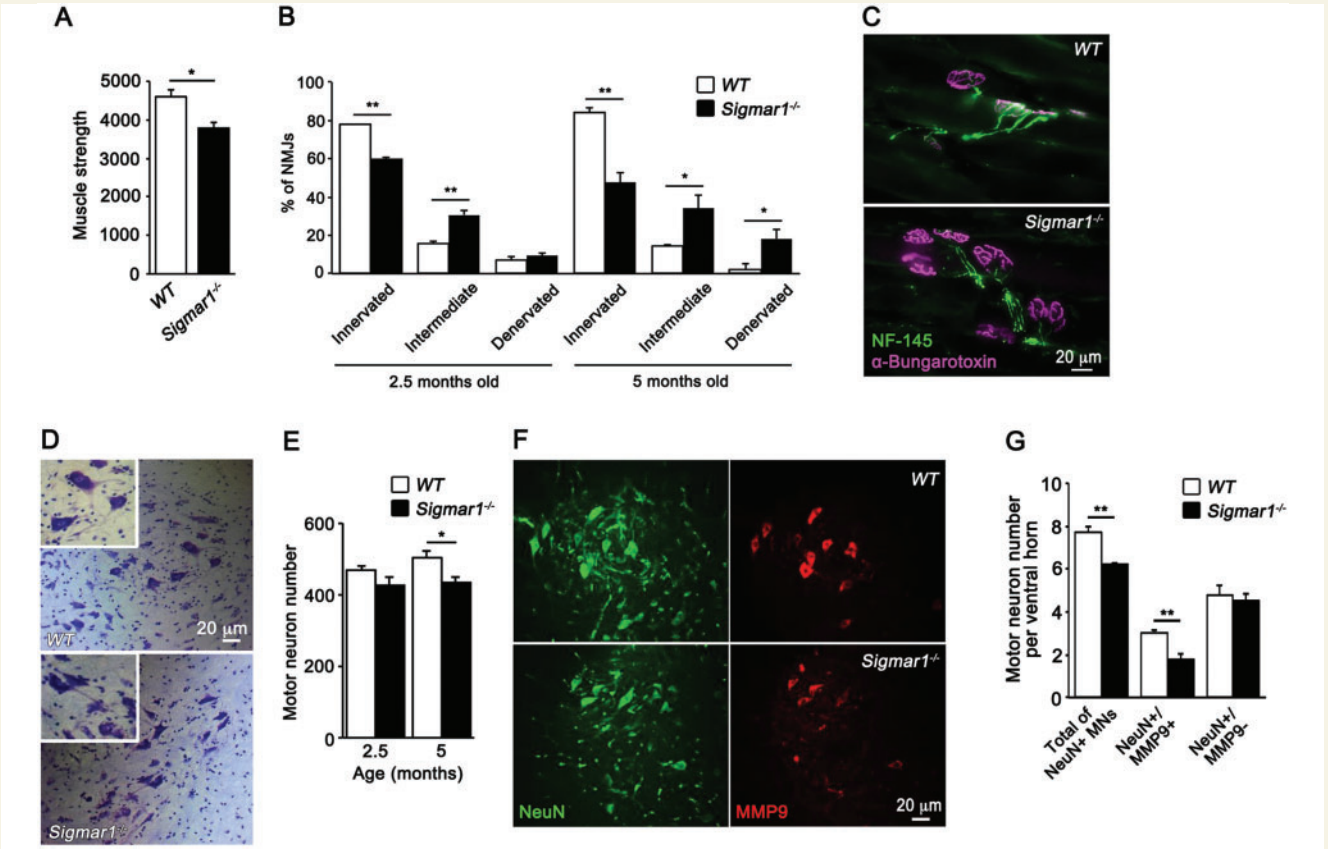

Figure 1 SIGMAR1 deficiency leads to motor neuron degeneration *in vivo*. (**A**) Grid test evaluation of muscle strength in 5-month-old wild-type ($n = 6$) and *Sigmar1*$^{-/-}$ ($n = 7$) mice. Values are expressed as mean score ± SEM. *$P < 0.05$. *P*-value represents the significance between the histogram bars under the two ends of the horizontal line above them. (**B**) Level of muscle innervation of tibialis anterior in wild-type and *Sigmar1*$^{-/-}$ mice (2.5- and 5-month-old) quantified by the co-localization between a nerve terminal marker (NF-145) and acetylcholine receptor (α-bungarotoxin). Results are expressed as the percentage of innervated, intermediate or denervated neuromuscular junctions/total of neuromuscular junctions ± SEM from $n = 3$ mice, *$P < 0.05$, **$P < 0.01$. (**C**) Examples of NF-145 and α-bungarotoxin staining of neuromuscular junctions (NMJ) in control (wild-type) and *Sigmar1*$^{-/-}$ preparations. (**D**) Section of spinal cord from wild-type and *Sigmar1*$^{-/-}$ mice stained by Nissl coloration. (**E**) Survival of motor neurons in lumbar portion of the spinal cord was evaluated on 44 spinal cord sections per mouse. (**F**) Section of spinal cord from 5 month-old wild-type and *Sigmar1*$^{-/-}$ mice stained for NeuN and MMP9 proteins. (**G**) Quantification of the number of MMP9 and NeuN positive motor neurons. The data are expressed as mean ± sem ($n = 4$ mice per genotype), *$P < 0.05$. MN = motor neuron.

oligonucleotides (and hence the targeted proteins) is <40 nm. As a control we applied only one of the two antibodies or we used antibodies targeting non-interacting proteins (anti-calreticulin, an ER protein, and anti-NeuN, a nuclear protein) (Fig. 3A). We did not observe any interactions (dots) under these conditions. The number of ITPR3–VDAC1 interactions were decreased both in the cell body and in axons of NE-100 treated and *Sigmar1*$^{-/-}$ motor neurons (cell body: NE-100: 61.3 ± 7.5% and *Sigmar1*$^{-/-}$: 51 ± 10%, axon: NE-100: 44.2 ± 17% and *Sigmar1*$^{-/-}$: 30.3 ± 7%, relative to their respective controls) as well as after thapsigargin treatment, which was previously shown to disturb mitochondria–ER connections (Goetz *et al.*, 2007) (Fig. 3A and B). In lumbar spinal cord of 2.5-month-old mice processed for electron microscopy, we evaluated, in motor neurons, the number of mitochondria apposed to the ER relative to the total number of mitochondria unapposed to the ER, per field. In controls, a mean fraction of ~30% of MAMs was observed whereas in *Sigmar1*$^{-/-}$ the MAMs fraction was ~18% (Fig. 3C and D).

Defective calcium homeostasis and ER stress activation contribute to neuronal degeneration linked to SIGMAR1 dysfunction

At the level of MAMs, ER transfers calcium towards the mitochondria and this is necessary for its metabolic function (Rizzuto *et al.*, 2012), and the disruption of MAM proteins is sufficient to induce calcium defects (De Vos *et al.*, 2012). We monitored the concentration of intracellular calcium, $[Ca^{2+}]_i$, using ratiometric Fura 2 imaging.

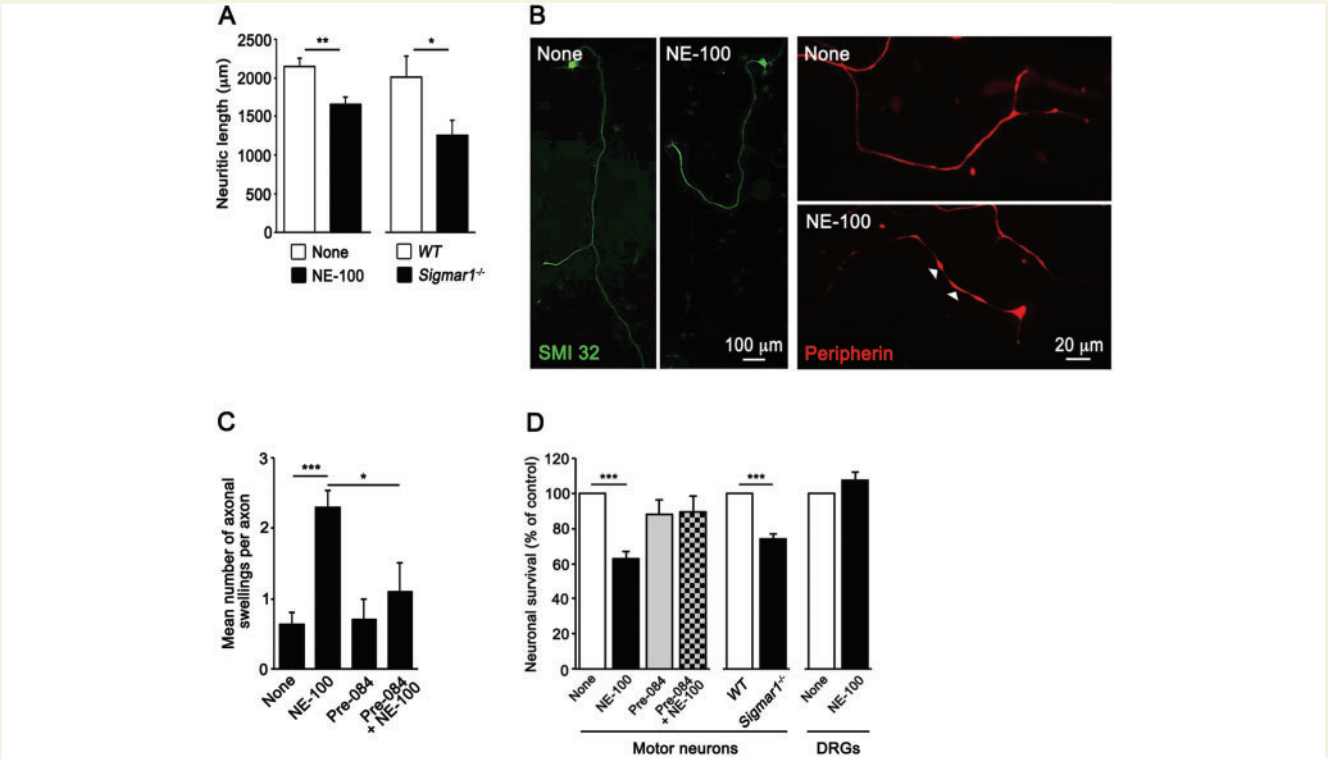

Figure 2 SIGMAR1 deficiency leads to motor neuron degeneration *in vitro*. (**A**) Wild-type, NE-100 treated and *Sigmar1*$^{-/-}$ motor neurons were stained with a specific motor neuron marker SMI32 and axonal length was measured using Neuron J plugin. Data are expressed as the mean ± SEM of three independent experiments. *$P < 0.05$, **$P < 0.01$, ***$P < 0.001$. (**B**) Examples of SMI32 and peripherin stainings of control and NE-100 treated motor neurons. (**C**) Number of axonal swellings per axons in wild-type, NE-100 (300 nM), Pre-084 (50 nM) or Pre-084 + NE-100 treated motor neurons. (**D**) Motor neuron and sensory neurons (dorsal root ganglias) survival was assayed 24 h after treatment of wild-type rat motor neurons with SIGMAR1 antagonist NE-100 (300 nM for motor neurons and 1 µM for dorsal root ganglia neurons) or agonist Pre-084 (50 nM) or 24 h after plating of mouse wild-type and *Sigmar1*$^{-/-}$ motor neurons. Data represent mean ± SEM of three independent experiments. *$P < 0.05$, **$P < 0.01$, ***$P < 0.001$.

To ensure that only viable cells were analysed, we induced a transient Ca^{2+} influx by depolarization with 25 mM KCl. Only cells that showed a transient increase in [Ca^{2+}]i were included in the analyses of resting [Ca^{2+}]i and decay time. In NE-100 treated motor neurons, resting [Ca^{2+}]i was significantly elevated (wild-type: 56 ± 0.07 nM, NE-100: 85 ± 0.2 nM) (Fig. 4A and B). We detected no significant difference between wild-type and NE-100 motor neurons in their response to the KCl stimulus (Fig. 4A). However, the time to return to basal levels was significantly longer (~20 s) in NE-100 treated motor neurons than in controls (Fig. 4C). These results suggest that inhibiting SIGMAR1 function dysregulated intracellular calcium homeostasis.

Because defects in calcium handling in motor neurons has been previously associated with ER stress activation (Bernard-Marissal *et al.*, 2012) and loss of SIGMAR1 function has been shown to induce ER dysfunction in cultured NSC-34 cells (Prause *et al.*, 2013), we analysed the level of expression of three ER stress indicators: phosphorylated EIF2A (phosphorylated following PERK activation), CHOP (C/EBP homologous protein, transcribed following PERK activation) and PDI in control and mutant conditions. These markers were significantly increased in NE-100 treated motor neurons and in *Sigmar1*$^{-/-}$ motor neurons as compared to their controls (Fig. 4D and E) but ER stress level was unchanged in dorsal root ganglia NE-100 treated neurons (Supplementary Fig. 2). As phosphorylated EIF2A is an early-activated ER stress marker we analysed its expression in lumbar spinal cord motor neurons of 2.5- and 5-month-old wild-type and *Sigmar1*$^{-/-}$ mice. We observed that phosphorylated EIF2A expression was strongly upregulated in spinal motor neurons of the *Sigmar1*$^{-/-}$ mice (Fig. 4D and F).

To determine whether the altered calcium homeostasis and ER stress play a functional role in motor neuron degeneration, motor neurons were cultured with or without NE-100 in combination or not with: a cytoplasmic calcium scavenger (BAPTA-AM), an ER stress inhibitor (salubrinal) or an inhibitor of the ER connected caspase-12 (Z-ATAD-fmk). The chelation of calcium and abrogation of ER stress significantly reduced axonal degeneration (NE-100: 1845 ± 230 µm, NE-100 + BAPTA-AM: 2424 ± 224 µm; NE-100 + salubrinal: 2495 ± 145 µm) (Fig. 4G) as well as

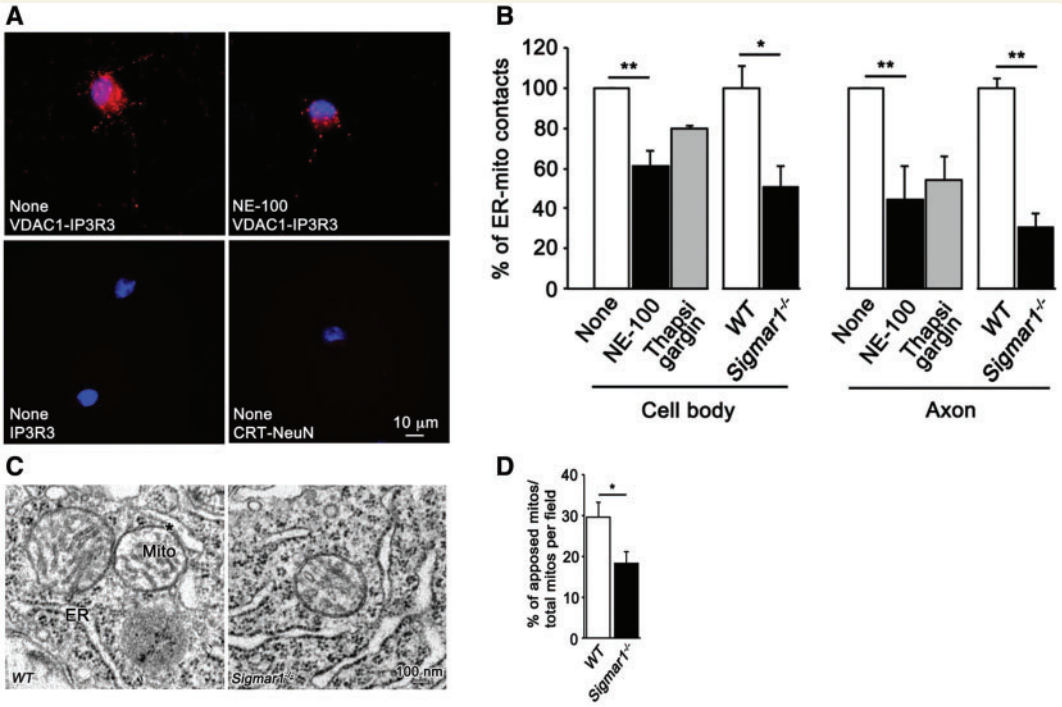

Figure 3 Inhibition and loss of SIGMAR1 function reduce contacts between mitochondria and ER in motor neurons both *in vitro* and *in vivo*. (**A**) Examples of mitochondria-ER contact analysis done *in vitro*, on purified motor neurons, using a proximity ligation assay. The red dots indicate proximity of the ER and mitochondria targeted respectively with an anti-ITPR3 (IP3R3) and anti-VDAC1 antibody. Anti-calreticulin (CRT) -anti-NeuN and anti-ITPR3 alone were used as negative controls. (**B**) Quantification of the proximity ligation assay results on wild-type, NE-100 (300 nM) and thapsigargin (10 nM) treated motor neurons and wild-type and *Sigmar1*$^{-/-}$ motor neurons. Data were analysed using Image J and expressed as percentage ± SEM relative to control ($n = 3$; *$P < 0.05$, **$P < 0.01$). (**C**) Examples of electron microscopy pictures of ER-mitochondria contacts in spinal motor neurons of wild-type and *Sigmar1*$^{-/-}$ mice. Asterisk indicates a MAM. (**D**) Quantification of mitochondria apposed on ER ($n = 3$ animals per genotype, *$P < 0.05$).

motor neuron death (NE-100: 60.3 ± 7.4%, NE-100 + BAPTA-AM: 80.7 ± 8%; NE-100 + salubrinal: 101.6 ± 7.6% and NE-100 + Z-ATAD-fmk: 94.8 ± 9.4%) (Fig. 4H).

We observed thus far that loss of function of SIGMAR1 compromises both calcium homeostasis and ER function leading to motor neuron degeneration. Both changes occur early (8 h after NE-100 treatment), but the relation between these two cellular defects remained unclear. We therefore measured intracellular calcium, $[Ca^{2+}]_i$ and phosphorylated EIF2A level in NE-100 treated motor neurons in combination or not of BAPTA-AM or salubrinal. Addition of either BAPTA-AM or salubrinal to motor neurons abrogated the increase of resting $[Ca^{2+}]$i observed in NE-100 condition leading to a $[Ca^{2+}]$i below control levels (wild-type: 58.2 ± 1.4 nM, NE-100: 98.02 ± 2.5 nM, NE-100 + BAPTA-AM: 40 ± 3.3 nM, NE-100 + salubrinal: 37.8 ± 1.3 nM) (Fig. 5A). The increase in phosphorylated EIF2A expression level observed in NE-100 was significantly reduced after salubrinal addition (wild-type: 100 ± 0 %, NE-100: 140.9 ± 10.7%, NE-100 + salubrinal: 57.5 ± 22) (Fig. 5B and C). However, the co-treatment of motor neurons with NE-100 and BAPTA-AM did not significantly change the expression of phosphorylated EIF2A compared to the NE-100 condition (Fig. 5B and C). These observations suggest that ER stress acts through calcium homeostasis impairment to trigger *Sigmar1*$^{-/-}$ motor neuron death.

Mitochondrial dysfunction is involved in the motor neuron degeneration process

At MAMs, ER tubules have been recently shown to circumscribe the mitochondria thus promoting mitochondrial fission (Westermann, 2011). Moreover, $[Ca^{2+}]$ regulates the level of phosphorylation of the key fission protein, the dynamin 1-like protein (Drp1, now known as DNM1L) (Dickey and Strack, 2011). To analyse mitochondrial morphology, we loaded motor neurons with MitoTracker® Red allowing us to target ~97% of axonal mitochondria (Supplementary Fig. 3C and D) and measure the mitochondrial length. We noticed a significant (~30%) increase in the mean mitochondrial size in both NE-100 treated and *Sigmar1*$^{-/-}$ motor neurons (Fig. 6A and B). The distribution of mitochondria according to their size highlights a significant increase in the proportion of mitochondria >3 µm in length (wild-type: 11 ± 3.3%, NE-100: 22 ± 2.4%). Conversely, a decrease in the proportion of

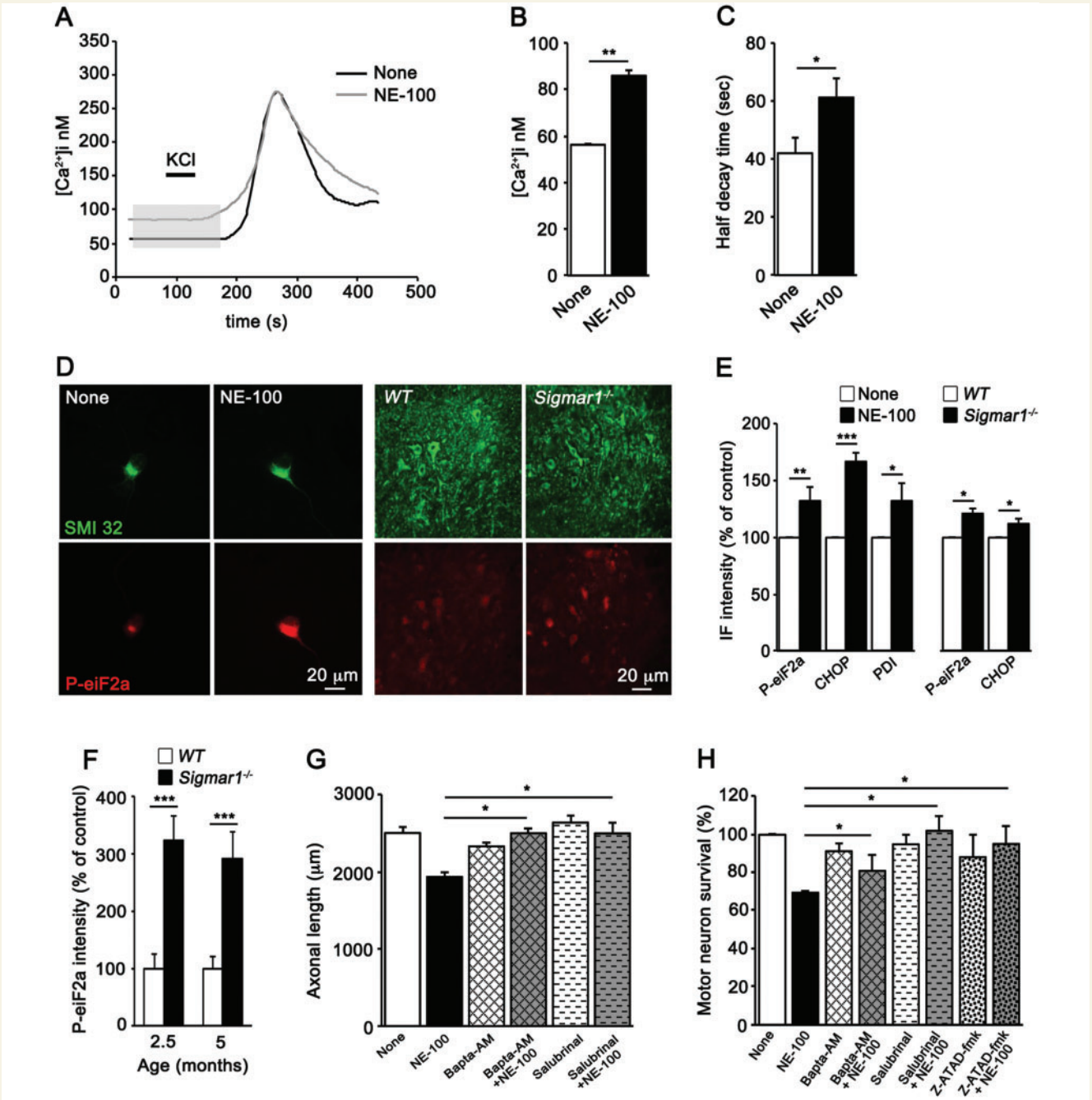

Figure 4 Calcium signalling and ER stress are involved in motor neuron degeneration induced by SIGMAR1 deficiency. (**A**) Intracellular calcium concentration $[Ca^{2+}]i$ was determined in motor neurons after 8 h of NE-100 treatment by Fura 2 ratio imaging. Resting $[Ca^{2+}]i$ was calculated for each individual neuron as the average resting $[Ca^{2+}]i$ between 30 and 180 s of measurement (grey box). (**B**) Representation of $[Ca^{2+}]i$ values determined by averaging the data obtained from individual cells. (**C**) Representation of half decay time (50% return to basal level) analysis. Data are from four experiments with ~20 neurons analysed per condition (values are mean ± SEM). (**D**) The level of ER stress was evaluated by marker phosphorylated EIF2A (P-eif2a) in cultured motor neurons (*left*) and on motor neurons of the lumbar spinal cord (*right*). (**E**) Wild-type rat motor neurons treated with NE-100 (300 nM) and cultured wild-type and *Sigmar1*$^{-/-}$ motor neurons were fixed and immunostained for ER stress markers (phosphorylated EIF2A, CHOP and PDI), in combination with a motor neuronal marker SMI32. The data represent mean intensity values of ER stress marker and are presented as a percentage change compared to control values arbitrarily set to 100%. (**F**) Phosphorylated EIF2A staining was used to quantify ER stress level in spinal motor neurons of 2.5 and 5-month-old wild-type and *Sigmar1*$^{-/-}$ mice and is represented as a change ± SEM compared to wild-type values arbitrarily set to 100%. (**G**) Motor neurons were treated with NE-100 (300 nM) in the presence or not of BAPTA-AM (5 µg/ml), a calcium chelator, or the ER stress inhibitor salubrinal. After 8 h of treatment, motor neurons were stained with SMI32 and axonal length was quantified. Values are mean ± SEM from three independent experiments, $^{*}P < 0.05$, $^{**}P < 0.01$. (**H**) Motor neurons were treated with NE-100 (300 nM) in combination or not with either BAPTA-AM, a calcium chelator, salubrinal (10 µM), an ER stress inhibitor or z-ATAD-fmk (10 µM), a caspase 12 inhibitor. Motor neuron survival was evaluated 24 h after treatment and expressed as percentage of control ± SEM. All data represent the mean of three independent experiments, $^{*}P < 0.05$, $^{**}P < 0.01$, $^{***}P < 0.001$.

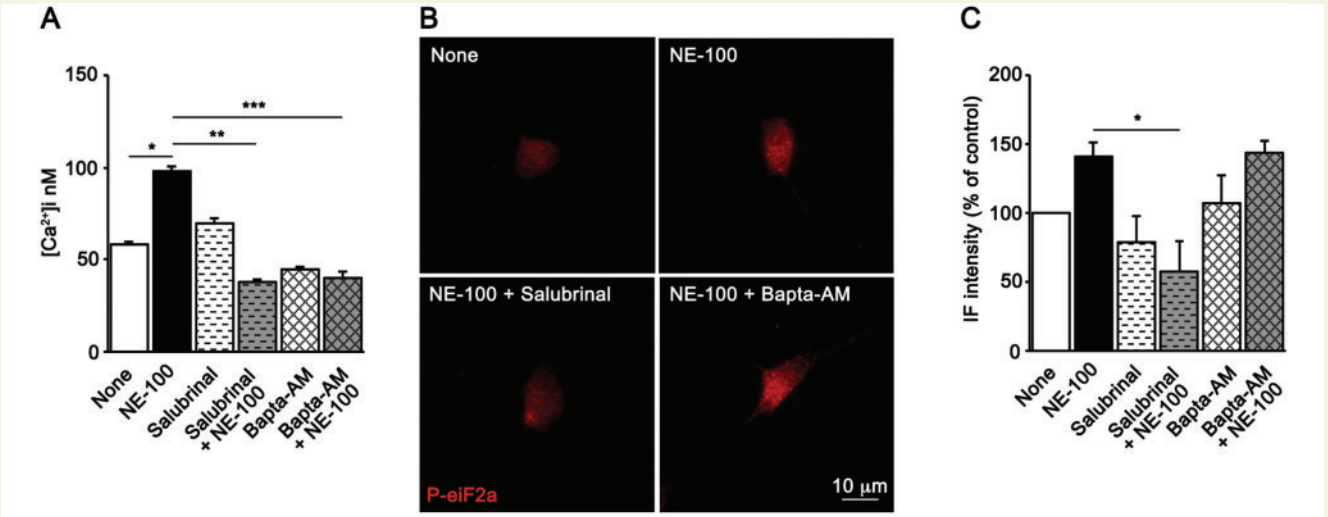

Figure 5 Evaluation of ER stress and calcium homeostasis crossregulation induced by SIGMAR1 deficiency. (**A**) Intracellular calcium concentration [Ca^{2+}]i was determined in motor neurons after 8 h of NE-100 (300 nM) in combination or not with salubrinal (10 µM) or BAPTA-AM (5 µg/ml) treatment by Fura 2 ratio imaging. Resting [Ca^{2+}]i was calculated for each individual neuron as the average resting [Ca^{2+}]i between 30 and 180 s of measurement. [Ca^{2+}]i values determined by averaging the data obtained from individual cells are represented. (**B**) The level of ER stress was evaluated by marker phosphorylated EIF2A in cultured motor neurons treated with NE-100 (300 nM) in combination or not with salubrinal (10µM) or BAPTA-AM (5 µg/ml). (**C**) The data represent mean intensity values of phosphorylated EIF2A and are presented as a percentage change compared to control values arbitrarily set to 100%. IF = immunofluorescence.

mitochondria of 1–2 µm in length was observed in cells treated with SIGMAR1 antagonist (wild-type: 54 ± 3.7%, NE-100: 38 ± 2.3%) (Fig. 6C). To determine whether the observed mitochondrial phenotype was a major effector in the axonal degeneration process in SIGMAR1 deficient motor neurons, we reproduced the size increase in mitochondria by using Mdivi-1, a selective inhibitor of DNM1L that blocks mitochondrial fission (Cassidy-Stone *et al.*, 2008). In motor neurons, mitochondrial length increases proportionally to Mdivi-1 concentration (Supplementary Fig. 3A and B). Importantly, when motor neurons were treated for 8 h with Mdivi-1 (10 µM), they showed a significant reduction in axonal length (Fig. 6D). At low doses (5 and 10 µM of Mdivi-1), motor neuron survival was of 80.7 ± 5.9% and 69.7 ± 0.8%, respectively relative to non-treated cells. At these concentrations we did not detect any changes in sensory neurons survival (Fig. 6E). At 20 µM, Mdivi-1 decreased motor neuron and sensory neurons survival by ~40% and 20%, respectively (Fig. 6E). These last data suggest that motor neurons are more sensitive to mitochondrial dysfunction than other neuronal types.

SIGMAR1 deficiency disrupts mitochondrial axonal transport

Defects in axonal transport of mitochondria have been observed in several models of motor neuron diseases and are usually connected to axonal degeneration (De Vos *et al.*, 2008). As we observed elongated mitochondria and axonal degeneration following SIGMAR1 dysfunction, we considered whether this could result in mitochondrial transport impairment. We performed time-lapse experiments on MitoTracker® Red loaded motor neurons and monitored mitochondrial transport in different conditions using a fully automated analysis with Difference Tracker plugin of ImageJ (Andrews *et al.*, 2010). We observed a significant decrease in the proportion of motile particles between non-treated (19 ± 1.3%) and NE-100 treated cultured neurons (15 ± 1.2%), and between wild-type (15.2 ± 1.8%) and *Sigmar1*$^{-/-}$ neurons (8.6 ± 1%) as well as in neurons treated with Mdivi-1 (14.6 ± 1.6%) (Fig. 7A and B). As a positive control we used monastrol, which specifically affects the anterograde transport by inhibiting kinesin 5 family proteins (Sunil *et al.*, 2012) leading to a decrease in motile particles in motor neurons (12 ± 1.4%) (Fig. 7B). Our additional more detailed study of mitochondrial movement showed a significant and specific decrease in the velocity of retrograde mitochondria in conditions of defective SIGMAR1 (Fig. 7C), which could explain the observed accumulation of distal mitochondria (Fig. 7D). Surprisingly, the inhibition of mitochondrial fission by Mdivi-1 does not affect mitochondrial velocity in any direction. This suggests that the dysregulation of retrograde mitochondrial transport could depend on other cellular mechanisms.

Calcium homeostasis defects and ER stress contribute to mitochondrial dysfunction

Intracellular calcium has been shown to influence mitochondrial motility by regulating the attachment of docking

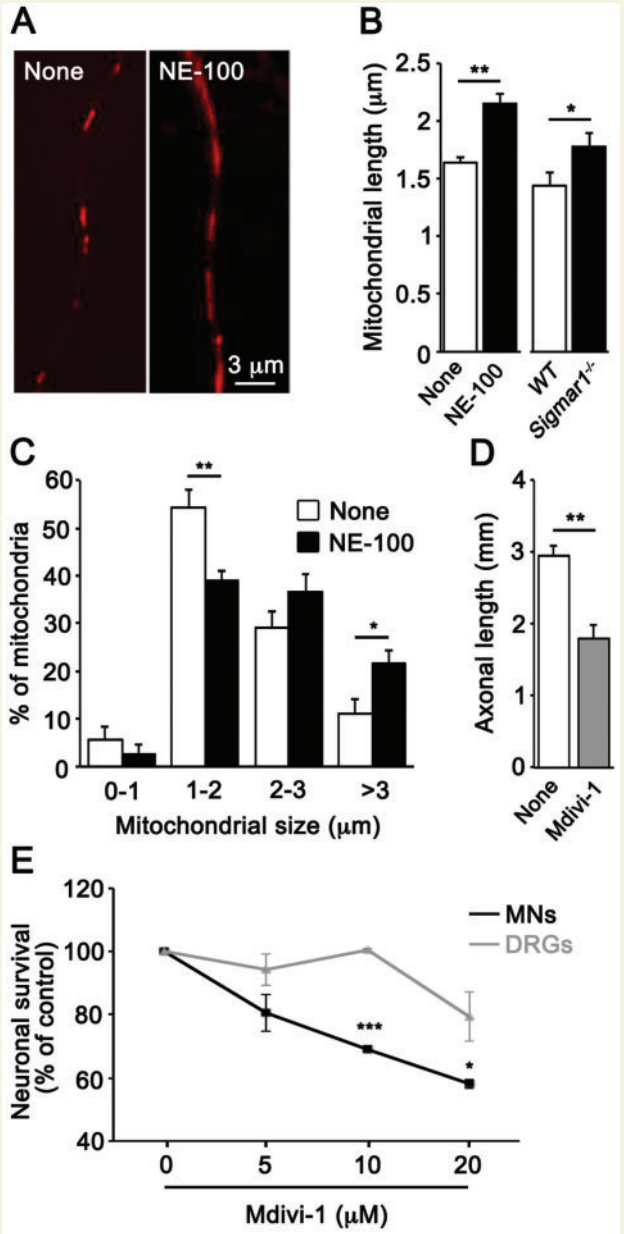

Figure 6 Deficit in mitochondrial dynamics induced by SIGMAR1 dysfunction triggers axonal degeneration and cell death. (**A**–**C**) NE-100 (300 nM) treated motor neurons or *Sigmar1*$^{-/-}$ motor neurons were loaded with MitoTracker® Red allowing staining of mitochondria. (**A**) Example of MitoTracker® Red-labelled mitochondria in control and NE-100 treated motor neurons. Mitochondrial length was measured in the proximal part of the axon and data were expressed as mean length of mitochondria (**B**) or expressed as a percentage of mitochondrial size category (**C**). (**D**) Axonal length was determined 8 h after Mdivi-1 treatment. Data represent the mean ± SEM. (**E**) Representation of motor neuron and sensory neurons survival after 24 h of treatment with various concentrations of Mdivi-1. Data are represented as percentage ± SEM relative to control. *$P < 0.05$, **$P < 0.01$, ***$P < 0.001$.

proteins Miro/Milton to motor proteins and microtubules (Sheng, 2014). As we noticed an increase in intracellular calcium associated with ER stress, we wondered whether these impairments can contribute to mitochondrial defects and motor neuron degeneration. After inhibiting SIGMAR1 function using NE-100, we treated motor neurons either with BAPTA-AM, a selective intracellular calcium chelator, or with an ER stress inhibitor salubrinal. The reduction in calcium overloading and ER stress level restored mitochondrial mean length (wild-type: 1.67 ± 0.11 µm, NE-100: 2.12 ± 0.14 µm, NE-100 + BAPTA-AM: 1.88 ± 0.05 µm, NE-100 + salubrinal: 1.7 ± 0.08 µm) (Fig. 8A). In recent studies, SIGMAR1 loss has been correlated to ER stress activation and an increase in unfolded protein response (Prause *et al.*, 2013). To determine whether the elongation of mitochondria depends on an ER stress as a result of protein unfolding or of ER calcium disturbance, we treated motor neurons with subtle doses of two well-known ER stress inducers: thapsigargin (5 nM), which depletes ER calcium stores and tunicamycin (0.5 µg/ml), which impairs ER protein folding (Bernard-Marissal *et al.*, 2012). Interestingly, mitochondrial length was significantly increased only after thapsigargin treatment (none: 1.58 ± 0.04 µm, thapsigargin: 2.12 ± 0.3 µm, tunicamycin: 1.64 ± 0.09 µm) (Fig. 8B). Addition of BAPTA-AM suppressed mitochondria elongation induced by thapsigargin (Fig. 8B). These data highlighted the importance of ER calcium homeostasis rather than ER protein folding in the modulation of mitochondria morphology. We also monitored mitochondria axonal transport in the presence or absence of BAPTA-AM (5 µg/ml). Enhancing calcium buffering was not able to improve the proportion of moving mitochondria; however, it restored the velocity of retrograde-moving mitochondria (Fig. 8C and D). This suggests that the observed protective effect on motor neuron survival after chelation of intracellular calcium may, in part, reduce motor neuron degeneration by increasing mitochondria velocity.

Discussion

In this study we focused on the role of one of the MAM proteins, SIGMAR1, in motor neuron function. SIGMAR1 disturbance have critical consequences in humans as pathogenic mutations in *SIGMAR1* have been identified in FTLD-ALS and juvenile ALS cases (Luty *et al.*, 2010; Al-Saif *et al.*, 2011). Here, we demonstrated that loss/impairment of SIGMAR1 leads to axonal and motor neuron degeneration both *in vitro* and *in vivo*. This was connected to MAM loss, calcium homeostasis impairment, ER stress activation, elongated mitochondria and defective mitochondrial transport.

In some models of motor neuron disease, motor neurons are thought to die through a dying-back degeneration process (Fischer *et al.*, 2004; Pun *et al.*, 2006). This phenomenon is initiated by a dysfunction of the axonal periphery,

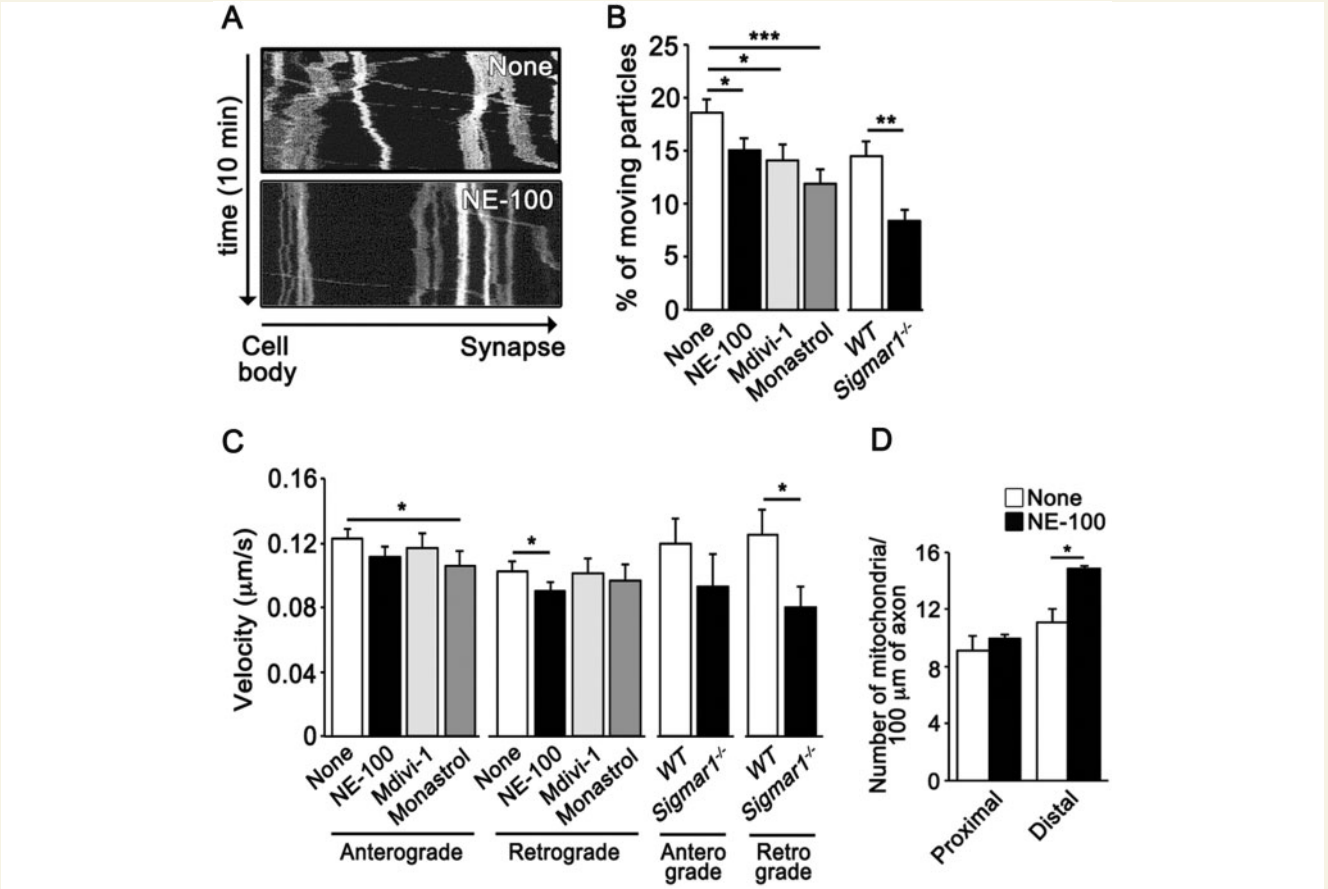

Figure 7 SIGMAR1 dysfunction disrupts mitochondrial axonal transport. (**A**) Representative kymographs show mitochondrial transport in control and NE-100 treated motor neurons. (**B**) The percentage of motility particles in control and NE-100, Mdivi-1 and monastrol treated motor neurons and in motor neurons isolated from control and *Sigmar1*$^{-/-}$ mice. (**C**) Anterograde and retrograde velocity of mitochondria was determined in depicted motor neuron cultures. Data are from five experiments with 25–35 neurons analysed, $*P < 0.05$. (**D**) Number of mitochondria in proximal and distal axonal segments was quantified in mitotracker-red loaded motor neurons treated or not with NE-100. Data were expressed as mean number of mitochondria per 100 µm of axon ± SEM. $*P < 0.05$.

which is followed by a progressive distal-to-proximal degeneration of the whole axon. In various models presented in this study, we observed features of axonal degeneration a long time before the loss of somas. In cultured motor neurons, axonal length was reduced as soon as 8 h after inhibition of SIGMAR1 with NE-100 or 16 h after plating of *Sigmar1*$^{-/-}$ motor neurons, whereas decrease in motor neuron survival was observed 24 h post-treatment or plating. Axonal length reduction probably reflects a process of axonal degeneration since we observed the presence of axonal swellings at the terminals of the axons as previously described in other motor neuron disease models (Selvaraj *et al.*, 2012).

Our behavioural characterization of *Sigmar1*$^{-/-}$ mice confirmed the previously described impairment in the rotarod test (Mavlyutov *et al.*, 2010). Interestingly, we also noticed a decrease in muscle strength in these mice scored by the grid test. In contrast to other motor neuron disease models such as the *SOD1*^{G93A} mice, the defects in the *Sigmar1*$^{-/-}$ mice are relatively subtle. Importantly, we connected for the first time the appearance of motor defects in *Sigmar1*$^{-/-}$ mice to neuromuscular dysfunction. Indeed, one-third of neuromuscular junctions were partially denervated in the fast-twitch muscle tibialis anterior at the age of 2.5 months, and 20% completely denervated at 5-months. Although we did not notice motor neuron death at 2.5 months, we observed a small but significant loss of motor neurons in the lumbar spinal cord of *Sigmar1*$^{-/-}$ mice at the age of 5 months. This last result was in line with a dying-back hypothesis in SIGMAR1 linked motor neuron degeneration. Interestingly, the slow-twitch muscle soleus of 5-month-old *Sigmar1*$^{-/-}$ mice was not affected, which may suggest a higher susceptibility of fast-fatigable fibres to degenerate as previously observed in other motor neuron disease models (Pun *et al.*, 2006). In agreement with this hypothesis, motor neurons highly expressing MMP9 were selectively lost in the ventral horn of 5-month-old *Sigmar1*$^{-/-}$ mice. Neuronal MMP9 was recently demonstrated as a determinant of the selective degeneration of fast vulnerable motor neurons in the *SOD1*^{G93A} ALS mouse

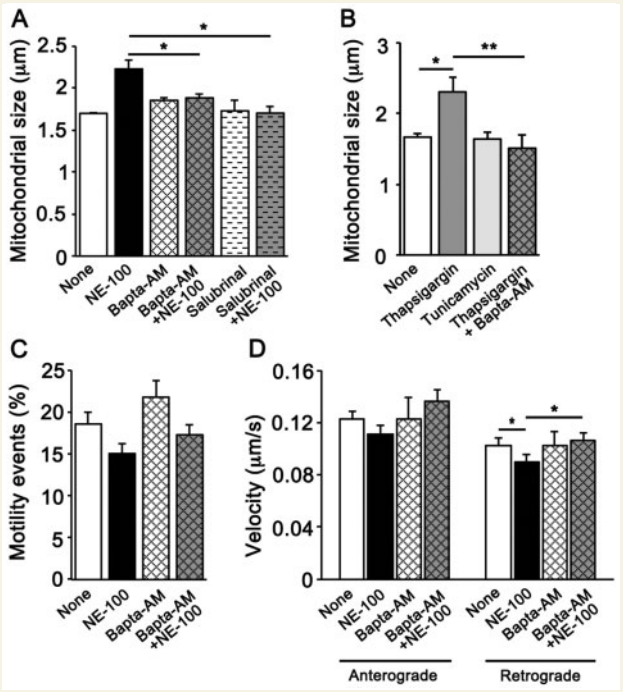

Figure 8 Intracellular calcium level and ER stress modulate various mitochondrial parameters in motor neurons. (**A**) Mitochondrial size was determined in motor neurons treated with NE-100 (300 nM) in presence or absence of BAPTA-AM (5 µg/ml) or salubrinal (10 µM). (**B**) Mitochondrial size was determined in motor neurons treated with two ER stress inducers thapsigargin (5 nM, ER calcium depletor) and tunicamycin (0.5 µg/ml, protein folding inhibitor) and the calcium chelator BAPTA-AM (5 µg/ml). (**C**) Motility events were quantified in motor neurons treated with NE-100 in combination with BAPTA-AM (5 µg/ml). (**D**) Mitochondrial velocity was quantified in motor neurons treated either with NE-100 or BAPTA-AM (5 µg/ml), then in combination with both. Data are expressed as means ± SEM. The data presented under 'None' and 'NE-100' are the same as in Fig. 7C. $^*P < 0.05$.

model (Kaplan *et al.*, 2014). Therefore our results suggest a role of SIGMAR1 in the vulnerability of a subpopulation of motor neurons.

At MAMs, SIGMAR1 is known to control calcium transfer from ER to the mitochondria by interacting with ITPR3 thus contributing to the stabilization of this receptor during elevated calcium transfer. In the absence of SIGMAR1, ITPR3 is prone to degradation and is thus unable to ensure proper calcium transfer (Hayashi and Su, 2007). We observed an important loss of contacts between the two organelles in motor neurons in the absence of SIGMAR1 as well as abnormalities in calcium homeostasis with, notably, an increase of basal calcium a few hours following SIGMAR1 inhibition and an increase in the time required to recover from KCl depolarization. These observations clearly indicate a defect in calcium extrusion and/or calcium buffering when SIGMAR1 function is affected. Interestingly, the deletion/mutation of other MAM protein-coding genes, such as *VAPB* and *MFN2* (mitofusin 2), has been shown to impair calcium homeostasis leading to a reduction of calcium mitochondria uptake, increase of intracellular calcium as well as ER calcium overload (de Brito and Scorrano, 2008; De Vos *et al.*, 2012), underlining the importance of MAMs in calcium homeostasis regulation. In parallel to calcium homeostasis defects, we observed an increase in ER stress following SIGMAR1 loss both *in vitro* and *in vivo*. Previous work connected the absence of SIGMAR1 chaperoning function to ER dysfunction and ER stress (Prause *et al.*, 2013). Surprisingly, inhibition of ER stress by salubrinal led to abrogated cytoplasmic calcium increase while the calcium chelator BAPTA-AM was not able to reduce ER stress level, placing ER stress upstream of calcium homeostasis defects. Besides its role in phosphorylated EIF2A dephosphorylation, salubrinal is known to upregulate ATF4 (Wu *et al.*, 2014). It is therefore possible that salubrinal modulates calcium level through the ATF4-anti apoptotic protein GRINA pathway, as previously demonstrated by Matus *et al.* (2013).

Under stress conditions, mitochondria maintain their function by dividing or fusing: mitochondrial fusion enables the exchange of contents between mitochondria, allowing defective mitochondria to regain components of the respiratory chain, whereas mitochondrial fission is required for proper mitochondrial transport and also facilitates apoptosis (Milone and Benarroch, 2012). We noticed an increase in mitochondrial length in axons of motor neurons following inhibition or loss of SIGMAR1. This increase did not result from a general increase of the length of all mitochondria but corresponded to a significant enrichment of very long mitochondria (with size >3 µm) concomitant to a loss of smaller mitochondria (<2 µm). Inducing artificially elongated mitochondria using a selective inhibitor of fission, Mdivi-1, was sufficient to induce axonal degeneration and motor neuron death. This observation supports the importance of a dysregulation of mitochondrial dynamics in SIGMAR1-linked motor neuron degeneration. This function is regulated by different types of dynamin-like guanosine triphosphate (GTP)-ases and indeed several of them have been found mutated or affected in different neurological disorders (Baxter *et al.*, 2002; Chung *et al.*, 2006; Waterham *et al.*, 2007). In particular, a dominant-negative mutation in DNM1L, which is involved in the mitochondrial fission process, has been associated with a fatal birth defect in humans (Waterham *et al.*, 2007). We did not notice a change in the level of expression/activation of DNM1L in our conditions (data not shown) suggesting the implication of other regulating fission/fusion protein(s) or other mechanisms. Alternatively, SIGMAR1 dysfunction could disturb the mitochondrial fission process via ER/mitochondrial disconnection. Indeed, the ER has been shown recently to participate in the mitochondrial fission process at MAMs by circumscribing the mitochondria (Westermann, 2011). We observed a reduction of mitochondria-ER connections both *in vitro* and *in vivo* in motor neurons deficient for SIGMAR1. The observed disconnection of the two organelles could

therefore reduce the efficiency of the mitochondrial fission process leading to hyperfused mitochondria.

In addition to mitochondrial fission and fusion defects, mitochondrial dysfunction has been previously linked to axonal transport alteration in various disorders (Misko *et al.*, 2012). Anterograde axonal transport allows bringing mitochondria to critical energy dependent sites, whereas retrograde transport takes care of driving mitochondria back to the cell body for repair or destruction. We observed that the SIGMAR1 inhibition in particular affects the retrograde mitochondrial velocity. Interestingly, in a mouse model of ALS, retrograde transport was reported to be selectively affected 2 months before the appearance of symptoms (Bilsland *et al.*, 2010). We observed an accumulation of mitochondria at the periphery of the axon, a phenomenon already identified *in vivo* in mice expressing a mutated form of the mitochondrial/MAM MFN2 protein (Cartoni *et al.*, 2010). It is possible that the observed mitochondrial accumulation reflects the consequence of the defects in retrograde transport.

Detected changes in mitochondrial size may reflect activation of a protective mechanism in SIGMAR1 affected motor neurons. Stress-induced mitochondrial hyperfusion was shown to increase ATP availability, avoiding mitophagy and promoting cell survival (Tondera *et al.*, 2009). However, it might be also a causative element in retrograde transport impairment because large mitochondria may be difficult to move back to the cell body for degradation and recycling. Previous studies done on cultured neurons expressing mutated MFN2 described defects in mitochondrial transport, a reduction in mitochondrial size and axonal degeneration (Misko *et al.*, 2010). Interestingly, the knockdown of OPA1, which disrupts mitochondrial fusion leading to generation of mitochondria with reduced size, was not sufficient to recapitulate axonal degeneration induced by presence of mutated MFN2 suggesting that the dysregulation of mitochondrial fusion is not sufficient to initiate axonal degeneration (Misko *et al.*, 2012). In our case, artificially increasing mitochondrial size by Mdivi-1 was sufficient to reproduce the consequence of the inhibition/loss of SIGMAR1 leading to a decreased proportion of moving mitochondria and axonal degeneration. These results are in accordance with previous literature showing that the inhibition of DNM1L results in enlarged mitochondria that are not localized properly in dendrites or axons (Kageyama *et al.*, 2012). Although inhibiting fission led to a decrease in the number of moving mitochondria, it did not impact the velocity of the population of moving mitochondria in any of the transport directions, contrary to changes induced by inhibition/loss of SIGMAR1.

The inhibition of fission induced by inhibition/loss of SIGMAR1 and Mdivi-1 treatment leads to an increase in the population of very elongated mitochondria ($>3\,\mu m$) that are probably not able to move at all. Interestingly, we observed that chelation of calcium restored the retrograde velocity of the remaining moving mitochondria, but did not rescue the number of moving mitochondria. Calcium level has been already shown to influence mitochondrial axonal transport by regulating the mitochondrial transport machinery via the mitochondrion adaptor Miro (Rizzuto *et al.*, 2012). Elevation of cytosolic calcium is thought to slow down moving mitochondria in the axons at sites lacking ATP. It is therefore possible that disturbed calcium homeostasis, which is a consequence of inhibition/loss of SIGMAR1 function, might account for the decrease of velocity of moving mitochondria.

In all experiments, we observed a specific degeneration of motor neurons following inhibition/loss of SIGMAR1 as compared to sensory neurons. Although SIGMAR1 has been previously shown to be expressed in myelinating glial cells (Palacios *et al.*, 2004) known to have a critical role in motor neuron survival (Lee *et al.*, 2012), we did not observe any defects in Schwann cell survival and proliferation under SIGMAR1 loss of function conditions (Supplementary Fig. 4A and B). Our results are in accordance with the phenotype of SIGMAR1 affected patients who display motor disabilities with no alteration of sensory functions or signs of demyelination (Luty *et al.*, 2010; Al-Saif *et al.*, 2011). This could be explained by a lower sensitivity of sensory neurons and Schwann cells to SIGMAR1 loss. Recent data demonstrated that the knock-down of SIGMAR1 in hippocampal neurons was sufficient to induce axonal degeneration but not the cell loss (Hedskog *et al.*, 2013). Similar differences were observed for other cell types: lens cells died after SIGMAR1 antagonist treatment whereas fibroblasts were resistant and it was proposed that cell sensitivity to calcium response following SIGMAR1 inhibition may underlie these differences (Spruce *et al.*, 2004; Wang and Duncan, 2006; Prause *et al.*, 2013). Motor neurons are known to be prone to degenerate following disturbance in calcium homeostasis. Their low content in calcium buffering proteins such as calreticulin has been recently demonstrated as a factor of their vulnerability both *in vitro* and *in vivo* (Bernard-Marissal *et al.*, 2015). Interestingly, calpastatin, an inhibitor of calcium-dependent cysteine protease, has been shown to reduce the toxicity of $SOD1^{G93A}$ in motor neurons *in vitro* (Tradewell and Durham, 2010).

Together, our results provide an important insight into the role of SIGMAR1 mediated ER–mitochondria interactions in motor neuron function. These findings may open new perspectives for the development of future therapies for patients with defects in SIGMAR1 function and more generally, in the field of motor neuron disease.

Acknowledgements

We wish to thank the electron microscopy facility (Faculty of Biology and Medicine, and the University Hospital, Lausanne, Switzerland) for help with ultrastructural analysis as well as the Centre for the study of behaviour (Faculty of Biology and Medicine, and the University Hospital, Lausanne, Switzerland) for the rotarod analysis.

Funding

This work was supported by grants from the Association Française contre les Myopathies (AFM to N.B-M.), Novartis Foundation for medical-biological research (to R.C.) from the Swiss National Science Foundation (SNSF to R.C., grant 31003A_135735/1) and from the Strategic Research Area Neuroscience (StratNeuro) Karolinska Institutet program (to R.C).

Supplementary material

Supplementary material is available at *Brain* online.

References

Al-Chalabi A, Jones A, Troakes C, King A, Al-Sarraj S, van den Berg LH. The genetics and neuropathology of amyotrophic lateral sclerosis. Acta Neuropathol 2012; 124: 339–52.

Al-Saif A, Al-Mohanna F, Bohlega S. A mutation in sigma-1 receptor causes juvenile amyotrophic lateral sclerosis. Ann Neurol 2011; 70: 913–9.

Andrews S, Gilley J, Coleman MP. Difference tracker: imageJ plugins for fully automated analysis of multiple axonal transport parameters. J Neurosci Methods 2010; 193: 281–7.

Baxter RV, Ben Othmane K, Rochelle JM, Stajich JE, Hulette C, Dew-Knight S, et al. Ganglioside-induced differentiation-associated protein-1 is mutant in Charcot-Marie-Tooth disease type 4A/8q21. Nat Genet 2002; 30: 21–2.

Bernard-Marissal N, Moumen A, Sunyach C, Pellegrino C, Dudley K, Henderson CE, et al. Reduced calreticulin levels link endoplasmic reticulum stress and Fas-triggered cell death in motoneurons vulnerable to ALS. J Neurosci 2012; 32: 4901–12.

Bernard-Marissal N, Sunyach C, Marissal T, Raoul C, Pettmann B. Calreticulin levels determine onset of early muscle denervation by fast motoneurons of ALS model mice. Neurobiol Dis 2015; 73: 130–6.

Bilsland LG, Sahai E, Kelly G, Golding M, Greensmith L, Schiavo G. Deficits in axonal transport precede ALS symptoms in vivo. Proc Natl Acad Sci USA 2010; 107: 20523–8.

Cartoni R, Arnaud E, Medard JJ, Poirot O, Courvoisier DS, Chrast R, et al. Expression of mitofusin 2(R94Q) in a transgenic mouse leads to Charcot-Marie-Tooth neuropathy type 2A. Brain 2010; 133 (Pt 5): 1460–9.

Cassidy-Stone A, Chipuk JE, Ingerman E, Song C, Yoo C, Kuwana T, et al. Chemical inhibition of the mitochondrial division dynamin reveals its role in Bax/Bak-dependent mitochondrial outer membrane permeabilization. Dev Cell 2008; 14: 193–204.

Chung KW, Kim SB, Park KD, Choi KG, Lee JH, Eun HW, et al. Early onset severe and late-onset mild Charcot-Marie-Tooth disease with mitofusin 2 (MFN2) mutations. Brain 2006; 129 (Pt 8): 2103–18.

Corbo M, Hays AP. Peripherin and neurofilament protein coexist in spinal spheroids of motor neuron disease. J Neuropathol Exp Neurol 1992; 51: 531–7.

Court FA, Coleman MP. Mitochondria as a central sensor for axonal degenerative stimuli. Trends Neurosci 2012; 35: 364–72.

Csordas G, Renken C, Varnai P, Walter L, Weaver D, Buttle KF, et al. Structural and functional features and significance of the physical linkage between ER and mitochondria. J Cell Biol 2006; 174: 915–21.

de Brito OM, Scorrano L. Mitofusin 2: a mitochondria-shaping protein with signaling roles beyond fusion. Antioxid Redox Signal 2008; 10: 621–33.

De Vos KJ, Grierson AJ, Ackerley S, Miller CC. Role of axonal transport in neurodegenerative diseases. Annu Rev Neurosci 2008; 31: 151–73.

De Vos KJ, Morotz GM, Stoica R, Tudor EL, Lau KF, Ackerley S, et al. VAPB interacts with the mitochondrial protein PTPIP51 to regulate calcium homeostasis. Hum Mol Genet 2012; 21: 1299–311.

Dickey AS, Strack S. PKA/AKAP1 and PP2A/Bbeta2 regulate neuronal morphogenesis via Drp1 phosphorylation and mitochondrial bioenergetics. J Neurosci 2011; 31: 15716–26.

Dierssen M, Arque G, McDonald J, Andreu N, Martinez-Cue C, Florez J, et al. Behavioral characterization of a mouse model overexpressing DSCR1/RCAN1. PLoS One 2011; 6: e17010.

Fischer LR, Culver DG, Tennant P, Davis AA, Wang M, Castellano-Sanchez A, et al. Amyotrophic lateral sclerosis is a distal axonopathy: evidence in mice and man. Exp Neurol 2004; 185: 232–40.

Goetz JG, Genty H, St-Pierre P, Dang T, Joshi B, Sauve R, et al. Reversible interactions between smooth domains of the endoplasmic reticulum and mitochondria are regulated by physiological cytosolic Ca2+ levels. J Cell Sci 2007; 120 (Pt 20): 3553–64.

Grynkiewicz G, Poenie M, Tsien RY. A new generation of Ca2+ indicators with greatly improved fluorescence properties. J Biol Chem 1985; 260: 3440–50.

Hayashi T, Rizzuto R, Hajnoczky G, Su TP. MAM: more than just a housekeeper. Trends Cell Biol 2009; 19: 81–8.

Hayashi T, Su TP. Sigma-1 receptor chaperones at the ER-mitochondrion interface regulate Ca(2+) signaling and cell survival. Cell 2007; 131: 596–610.

Hedskog L, Pinho CM, Filadi R, Ronnback A, Hertwig L, Wiehager B, et al. Modulation of the endoplasmic reticulum-mitochondria interface in Alzheimer's disease and related models. Proc Natl Acad Sci USA 2013; 110: 7916–21.

Kageyama Y, Zhang Z, Roda R, Fukaya M, Wakabayashi J, Wakabayashi N, et al. Mitochondrial division ensures the survival of postmitotic neurons by suppressing oxidative damage. J Cell Biol 2012; 197: 535–51.

Kaplan A, Spiller KJ, Towne C, Kanning KC, Choe GT, Geber A, et al. Neuronal matrix metalloproteinase-9 is a determinant of selective neurodegeneration. Neuron 2014; 81: 333–48.

Langa F, Codony X, Tovar V, Lavado A, Gimenez E, Cozar P, et al. Generation and phenotypic analysis of sigma receptor type I (sigma 1) knockout mice. Eur J Neurosci 2003; 18: 2188–96.

Lee Y, Morrison BM, Li Y, Lengacher S, Farah MH, Hoffman PN, et al. Oligodendroglia metabolically support axons and contribute to neurodegeneration. Nature 2012; 487: 443–8.

Luty AA, Kwok JB, Dobson-Stone C, Loy CT, Coupland KG, Karlstrom H, et al. Sigma nonopioid intracellular receptor 1 mutations cause frontotemporal lobar degeneration-motor neuron disease. Ann Neurol 2010; 68: 639–49.

Mancuso R, Olivan S, Rando A, Casas C, Osta R, Navarro X. Sigma-1R agonist improves motor function and motoneuron survival in ALS mice. Neurotherapeutics 2012; 9: 814–26.

Matus S, Lopez E, Valenzuela V, Nassif M, Hetz C. Functional contribution of the transcription factor ATF4 to the pathogenesis of amyotrophic lateral sclerosis. PLoS One 2013; 8: e66672.

Mavlyutov TA, Epstein ML, Andersen KA, Ziskind-Conhaim L, Ruoho AE. The sigma-1 receptor is enriched in postsynaptic sites of C-terminals in mouse motoneurons. An anatomical and behavioral study. Neuroscience 2010; 167: 247–55.

Mavlyutov TA, Epstein ML, Verbny YI, Huerta MS, Zaitoun I, Ziskind-Conhaim L, et al. Lack of sigma-1 receptor exacerbates ALS progression in mice. Neuroscience 2013; 240: 129–34.

Milone M, Benarroch EE. Mitochondrial dynamics: general concepts and clinical implications. Neurology 2012; 78: 1612–9.

Misko A, Jiang S, Wegorzewska I, Milbrandt J, Baloh RH. Mitofusin 2 is necessary for transport of axonal mitochondria and interacts with the Miro/Milton complex. J Neurosci 2010; 30: 4232–40.

Misko AL, Sasaki Y, Tuck E, Milbrandt J, Baloh RH. Mitofusin2 mutations disrupt axonal mitochondrial positioning and promote axon degeneration. J Neurosci 2012; 32: 4145–55.

Ono Y, Tanaka H, Takata M, Nagahara Y, Noda Y, Tsuruma K, et al. SA4503, a sigma-1 receptor agonist, suppresses motor neuron damage in *in vitro* and *in vivo* amyotrophic lateral sclerosis models. Neurosci Lett 2014; 559: 174–8.

Palacios G, Muro A, Verdu E, Pumarola M, Vela JM. Immunohistochemical localization of the sigma1 receptor in Schwann cells of rat sciatic nerve. Brain Res 2004; 1007: 65–70.

Prause J, Goswami A, Katona I, Roos A, Schnizler M, Bushuven E, et al. Altered localization, abnormal modification and loss of function of Sigma receptor-1 in amyotrophic lateral sclerosis. Hum Mol Genet 2013; 22: 1581–600.

Pun S, Santos AF, Saxena S, Xu L, Caroni P. Selective vulnerability and pruning of phasic motoneuron axons in motoneuron disease alleviated by CNTF. Nat Neurosci 2006; 9: 408–19.

Rizzuto R, De Stefani D, Raffaello A, Mammucari C. Mitochondria as sensors and regulators of calcium signalling. Nat Rev Mol Cell Biol 2012; 13: 566–78.

Saxena S, Cabuy E, Caroni P. A role for motoneuron subtype-selective ER stress in disease manifestations of FALS mice. Nat Neurosci 2009; 12: 627–36.

Selvaraj BT, Frank N, Bender FL, Asan E, Sendtner M. Local axonal function of STAT3 rescues axon degeneration in the pmn model of motoneuron disease. J Cell Biol 2012; 199: 437–51.

Sheng ZH. Mitochondrial trafficking and anchoring in neurons: New insight and implications. J Cell Biol 2014; 204: 1087–98.

Spruce BA, Campbell LA, McTavish N, Cooper MA, Appleyard MV, O'Neill M, et al. Small molecule antagonists of the sigma-1 receptor cause selective release of the death program in tumor and self-reliant cells and inhibit tumor growth *in vitro* and *in vivo*. Cancer Res 2004; 64: 4875–86.

Sreedharan J, Brown RH, Jr. Amyotrophic lateral sclerosis: Problems and prospects. Ann Neurol 2013; 74: 309–16.

Stendel C, Roos A, Kleine H, Arnaud E, Ozcelik M, Sidiropoulos PN, et al. SH3TC2, a protein mutant in Charcot-Marie-Tooth neuropathy, links peripheral nerve myelination to endosomal recycling. Brain 2010; 133 (Pt 8): 2462–74.

Sunil N, Lee S, Shea TB. Interference with kinesin-based anterograde neurofilament axonal transport increases neurofilament-neurofilament bundling. Cytoskeleton 2012; 69: 371–9.

Tondera D, Grandemange S, Jourdain A, Karbowski M, Mattenberger Y, Herzig S, et al. SLP-2 is required for stress-induced mitochondrial hyperfusion. EMBO J 2009; 28: 1589–600.

Tradewell ML, Durham HD. Calpastatin reduces toxicity of SOD1G93A in a culture model of amyotrophic lateral sclerosis. Neuroreport 2010; 21: 976–9.

Wang L, Duncan G. Silencing of sigma-1 receptor induces cell death in human lens cells. Exp Cell Res 2006; 312: 1439–46.

Waterham HR, Koster J, van Roermund CW, Mooyer PA, Wanders RJ, Leonard JV. A lethal defect of mitochondrial and peroxisomal fission. N Engl J Med 2007; 356: 1736–41.

Westermann B. Organelle dynamics: ER embraces mitochondria for fission. Curr Biol 2011; 21: R922–4.

Wu L, Luo N, Zhao HR, Gao Q, Lu J, Pan Y, et al. Salubrinal protects against rotenone-induced SH-SY5Y cell death via ATF4-parkin pathway. Brain Res 2014; 1549: 52–62.